



# Obrabotka metallov - Metal Working and Material Science

Journal homepage: [http://journals.nstu.ru/obrabotka\\_metallov](http://journals.nstu.ru/obrabotka_metallov)



## The structure, phase composition, and residual stresses of diffusion boride layers formed by thermal-chemical treatment on the die steel surface

Undrakh Mishigdorzhiiyn<sup>1, 2, a, \*</sup>, Nikolay Ulakhanov<sup>2, 1, b</sup>, Aleksandr Tikhonov<sup>3, 2, c</sup>, Pavel Gulyashinov<sup>4, 2, d</sup>

<sup>1</sup> Institute of Physical Material Science of the Siberian Branch of the RAS, 6 Sakhyanovoy str., Ulan-Ude, 670047, Russian Federation

<sup>2</sup> East Siberia State University of Technology and Management, 40V Kluchevskaya str, Ulan-Ude, 670013, Russian Federation

<sup>3</sup> Irkutsk National Research Technical University, 83 Lermontov str., Irkutsk, 664074, Russian Federation

<sup>4</sup> Baikal Institute of Nature Management Siberian branch of the Russian Academy of sciences, 6 Sakhyanovoy str., Ulan-Ude, 670047 Russian Federation

<sup>a</sup>  <https://orcid.org/0000-0002-7863-9045>,  [undrakh@ipms.bsnet.ru](mailto:undrakh@ipms.bsnet.ru), <sup>b</sup>  <https://orcid.org/0000-0002-0635-4577>,  [nulahanov@mail.ru](mailto:nulahanov@mail.ru),

<sup>c</sup>  <https://orcid.org/0000-0002-4917-9916>,  [tihonovalex90@mail.ru](mailto:tihonovalex90@mail.ru), <sup>d</sup>  <https://orcid.org/0000-0001-6776-9314>,  [gulpasha@mail.ru](mailto:gulpasha@mail.ru).

### ARTICLE INFO

#### Article history:

Received: 18 mart 2021

Revised: 05 April 2021

Accepted: 17 April 2021

Available online: 15 June 2021

#### Keywords:

Thermal-chemical treatment (TCT)

Surface layer quality

Boriding

Residual stresses

Structural state

Phase composition

Die steel

#### Funding

The research was supported by a grant from the Russian Science Foundation (project 19-79-10163).

#### Acknowledgements

The authors are grateful to Svetlana Mantstova for translation the English-language section of the paper.

### ABSTRACT

**Introduction.** Control and management of technological residual stresses (TRS) are among the most critical mechanical engineering technology tasks. Boriding can provide high physical and mechanical properties of machine parts and tools with minimal impact on the stress state in the surface layers. **The purpose of this work** is to determine the temperature modes of diffusion boriding, contributing to a favorable distribution of TRS in the surface layer of die steel 3Kh2V8F. The paper considers the results of studies on the TRS determination by the experimental method on the UDION-2 installation in diffusion layers on the studied steel surface. Boriding was carried out in containers with a powder mixture of boron carbide and sodium fluoride as an activator at a temperature of 950 °C and 1050 °C for 2 hours. The obtained samples of steels with a diffusion layer were examined using an optical microscope and a scanning electron microscope (SEM); determined the layers' microhardness, elemental, and phase composition. The experiments resulted in the following findings: as the boriding temperature rose from 950 °C to 1050 °C, the diffusion layer's thickness increased from 20 to 105 μm. The low-temperature mode of thermal-chemical treatment (TCT) led to the formation of iron boride Fe<sub>2</sub>B with a maximum boron content of 6 % and a microhardness up to 1250 HV. A high-temperature mode resulted in FeB formation with a top boron content of 11 % and a microhardness up to 1880 HV. **Results and Discussions.** It is found that boriding at 950 °C led to a more favorable distribution of compression TRS in the diffusion layer. However, significant TRS fluctuations in the diffusion layer and the adjacent (transitional) zone could affect the operational properties after TCT at a given temperature. An increase in the TCT temperature led to tensile TRS's appearance in the layer's upper zone at a depth of up to 50 μm from the surface. Despite tensile stresses on the diffusion layer surface after high-temperature TCT, the distribution of TCT is smoother than low-temperature boriding.

**For citation:** Mishigdorzhiiyn U.L., Ulakhanov N.S., Tikhonov A.G., Gulyashinov P.A. The structure, phase composition, and residual stresses of diffusion boride layers formed by thermal-chemical treatment on the die steel surface. *Obrabotka metallov (tekhnologiya, oborudovanie, instrumenty) = Metal Working and Material Science*, 2021, vol. 23, no. 2, pp. 147–162. DOI: 10.17212/1994-6309-2021-23.2-147-162. (In Russian).

#### \* Corresponding author

Mishigdorzhiiyn Undrakh L., Ph.D. (Engineering), Head of the laboratory  
 Institute of Physical Material Science of the Siberian Branch of the RAS  
 6 Sakhyanovoy str.,  
 670047, Ulan-Ude, Russian Federation  
 Tel.: 8 (3012) 43-48-70, e-mail: undrakh@ipms.bsnet.ru

## Introduction

The quality of the surface layer of machine parts and tools is determined by many parameters (roughness, waviness, hardness, residual stresses, etc.). It is ensured by a sequence of mechanical and heat treatment operations. Thermal-chemical treatment (TCT) of metals is used to harden the surface layers of forming tools, such as dies for stamping processes and injection molding [1-4]. In this case, the technological equipment durability and the quality of the products made with its help depend on the quality of the obtained diffusion layers. That determines the need for an integrated approach to assess the properties of diffusion layers, including its' physical and mechanical properties, structural, phase, and stress state.

It is evident that after TCT there is a difference in the specific volumes of the diffusion layer and the base steel, under the influence of which residual stresses (RS) arise, which have a significant effect on the performance of the coating and the product as a whole. It is known that compressive RS are more preferable in terms of fatigue crack retardation, which is also true for TCT processes [5, 6]. Thus, the authors [6, 7] found out that the processes of carburizing, nitriding, boriding, and borosiliconizing positively affect the distribution of RS on alloy structural steel (0.25 % C, 0.8 % Mn, 0.03 % Ti), and VKS-5, EP718, VNS-17 alloys.

RS measurement by Davydenkov's method for combined processes, including carburizing and subsequent grinding of 17CrNi6-6 alloy steel (EN 10084-2008 standard), is considered in [8]. The authors discovered that common and low-temperature carburizing leads to a favorable distribution of RS in the diffusion layer. Subsequent fine grinding with a CBN grinding wheel made it possible to maintain the RS distribution. A positive effect of this tool on the roughness of die steel (0.3 % C, 2 % Cr, 8 % W, 0.2 % V) after boroaluminizing is well known [9]. Thus, the initial roughness after TCT was reduced from 7.7  $\mu\text{m}$  to 0.43  $\mu\text{m}$  in terms of the  $R_a$  parameter. In the research [10, 11], the results of a favorable distribution of RS in the diffusion layer after combined treatment, including boriding followed by ultrasonic treatment of carbon steel, are also presented.

Thus, when developing methods for diffusion treatment on the surface of steel products it is necessary to focus on such RS distributions that ensure the desired performance properties of the machine units. A literature review of recent publications on the RS revealed a lack of publications on the RS determination after die steel (0.3 % C, 2 % Cr, 8 % W, 0.2 % V) boriding.

This work aims to determine the diffusion boriding temperature, which contributes to a favorable RS distribution in the surface layer of die steel (0.3 % C, 2 % Cr, 8 % W, 0.2 % V).

## Methodology

Samples of die steel (0.3 % C, 2 % Cr, 8 % W, 0.2 % V) (Table 1) were subjected to TCT in powder mixtures using furnace heating.

The powder method was carried out in containers with a fusible seal (Fig. 1) [12]. The parts were packed in a container with a fusible glass sealed lid. The container was then loaded into a preheated furnace. After the exposure, the container was cooled outside the furnace in still air.

Boriding was carried out in a powder mixture of boron carbide and sodium fluoride as an activator (96 %  $\text{B}_4\text{C}$  + 4 % NaF) at 950 °C and 1050 °C for 2 hours.

The microstructure was investigated using optical and scanning electron microscopy (SEM). The microhardness was determined using a PMT-3M microhardness tester at a load of 100 gf. EDS analysis was carried out on the JSM-6510LV JEOL SEM with an INCA Energy 350 microanalysis system at an

Table 1

Chemical composition of 3Kh2V8F/3X2B8 $\Phi$  steel, wt. %

C	Si	Mn	P	S	Cr	Ni	Cu	W	V
0.3–0.4	0.15–0.4	0.15–0.4	> 0.03	> 0.03	2.2–2.7	> 0.35	> 0.03	8.5–10.0	0.3–0.6

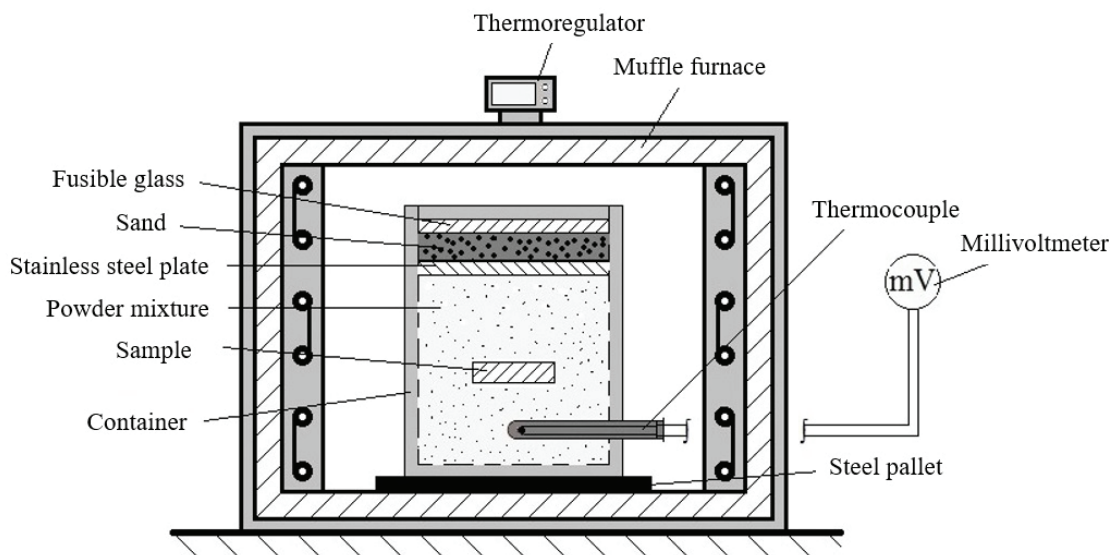


Fig. 1. Parts packing scheme for saturation from powder mixtures

accelerating voltage of 10 keV in SE mode at the Research Center “Progress”, ESSUTM. EDS analysis results were presented with an accuracy of tenths of a percent. In this case, the error probability was 1–5 % by weight. Phase analysis was carried out on a D8 ADVANCE Bruker X-ray diffractometer in copper radiation with an interval of 10–70° at the Research Center of BINM SB RAS.

RS in boride layers after TCT were measured using a UDION-2 installation for RS testing by a mechanical method, which was developed at INITU (Fig. 2) [13, 14].

The research focuses on the subsurface RS measurement as the main source of the mechanical components’ destruction.

The RS examination was carried out on flat samples such as plates. This mechanical method for RS determining upon this particular shape is also known as a strip method. The method is a procedure of the samples’ deformations recording during continuous removal of stressed zones depending on the thickness of the removed layer. Strain gauges with a data collection system were used to register the samples’ deformation and electrochemical etching or anodic dissolution was used to remove layer from the samples.

Elementary strip samples were prepared to determine the RS after TCT, (Fig. 3).

Dimension parameters of the sample strips (thickness  $h$  and width  $b$ ) were measured, as well as its initial deformations (deflection arrow  $f^0$ ) (Fig. 5) necessary for the subsequent RS calculation. Then the samples were dipped into protective rubber enamel and dried. After drying, the protective enamel was removed from the investigated surface by a blade in a rectangular shape of 30 mm long and with the same width as the strip.

A two-armed lever was mounted to one end of the sample strip to transmit deformations to strain gauges, while the other end of the sample was fixed to the bracket of the metrological frame of the UDION-2 installation (Fig. 4).

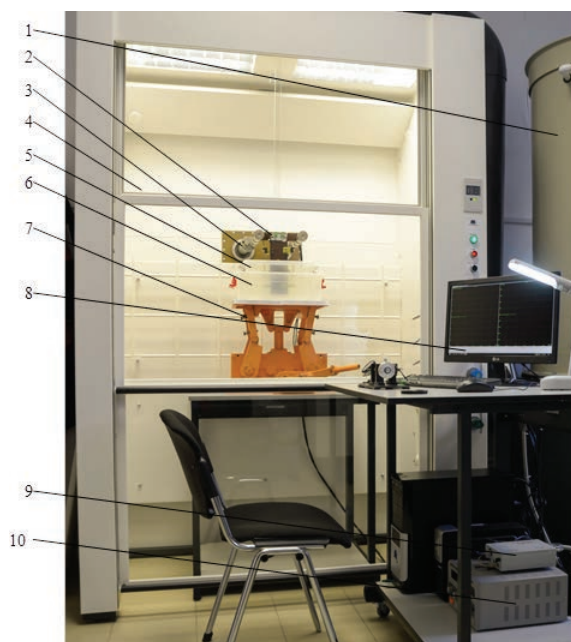


Fig. 2. Installation UDION-2/УДИОН-2 for measuring residual stresses by mechanical method: 1 – scrubber; 2 – device for sample fixing (metrological frames); 3 – bracket; 4 – fume hood; 5 – bath with electrolyte solution; 6 – thermostatic bath; 7 – bath lifting device; 8 – personal computer; 9 – strain gauge modules of the data collection system; 10 – electrochemical circuit power supply

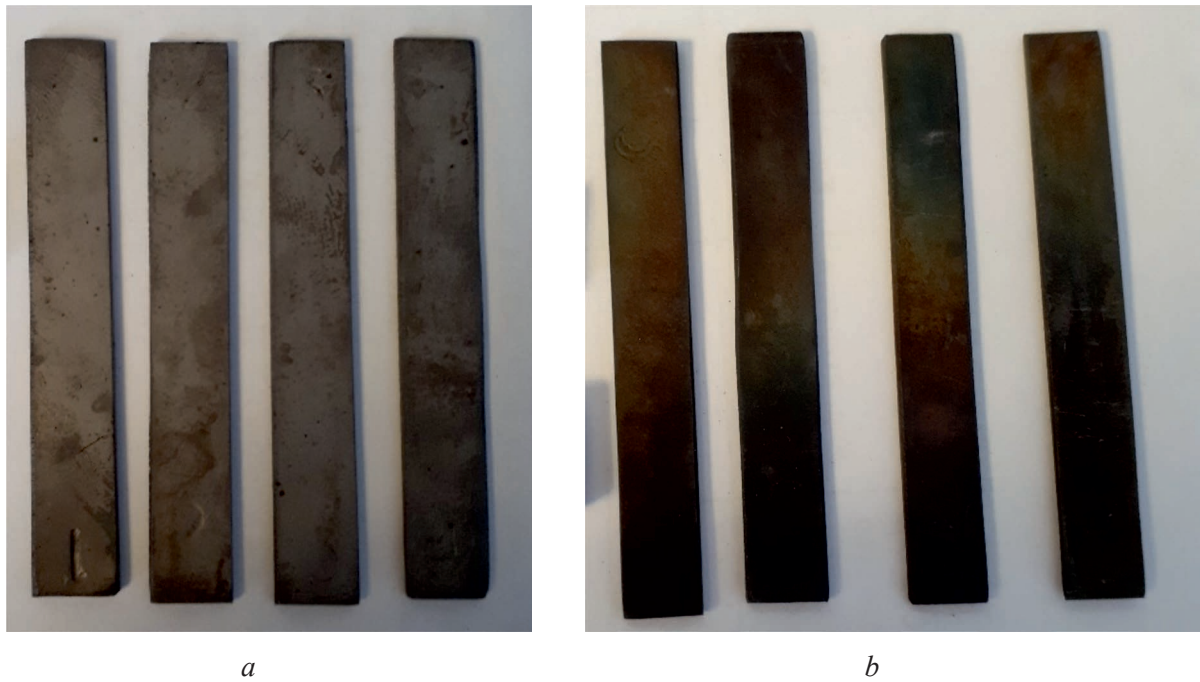


Fig. 3. Samples-strips after boriding for determination of residual stresses by mechanical method:  
*a* – 950 °C, 2 h; *b* – 1050 °C, 2 h

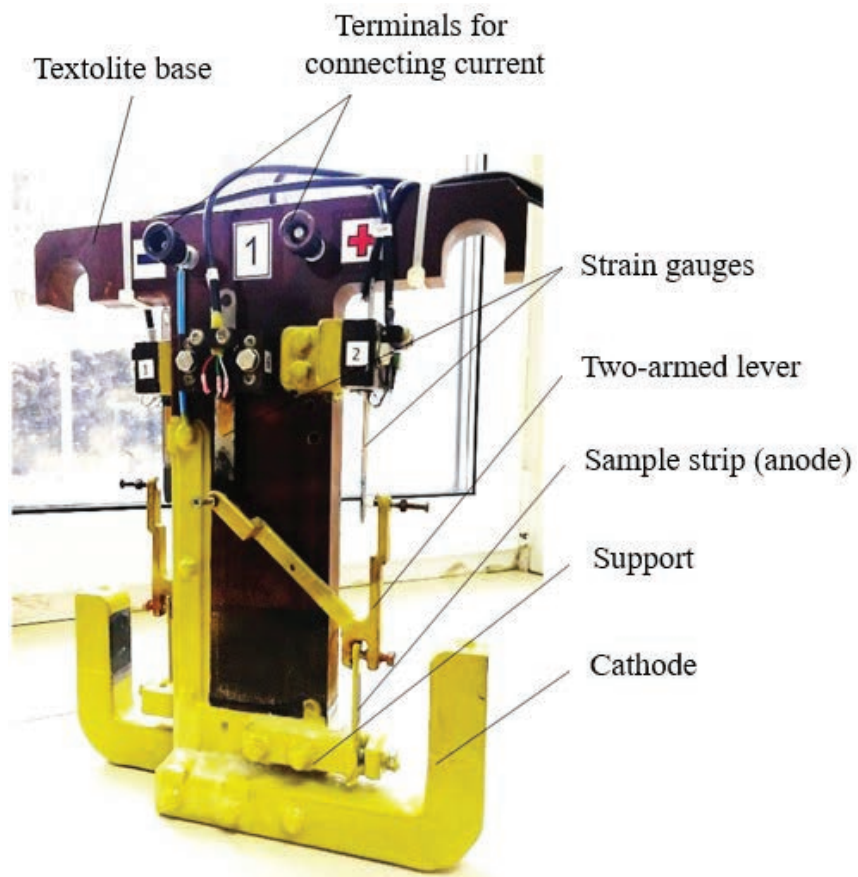


Fig. 4. The device (metrological frame) of the UDION-2/УДИОН-2 installation for the study of residual stresses in flat samples during the electrochemical method of removing layers

Metrological frames with the samples were installed and fixed in a fume hood on brackets above a bath with electrolyte solution, set up on the stage of the lifting device (Fig. 2). The strain gauges were connected to the LTR-EU-2-5 “L Card” Data Acquisition System (DAS). The Mastech HY3010 current source was connected to the terminals.

DAS of the UDION-2 installation controlled by the ACTest software provides obtaining, processing, visualization, and storing information from the strain gauges during the experiment. The processed information obtained from the strain gauges and the measured parameters of the samples, essential for the subsequent RS calculation, were stored in the database “Parameters of the UDION samples”.

After preparatory operations, the experiment was launched: the supply and exhaust ventilation system were switched on, the test scenario was activated, the stage of the lifting mechanism with the baths was raised so that the samples were completely immersed in the solution. The current source was switched on and the DAS was started, layer-by-layer electrochemical etching (anodic dissolution) was performed. The composition of the electrolyte used and the modes of anodic dissolution are shown in Table 2.

Table 2

**Electrolyte composition and parameters for electrochemical etching (anodic dissolution) of samples after chemical heat treatment**

Electrolyte composition (g/l)	$t, ^\circ\text{C}$	Current density $j, \text{A} / \text{dm}^2$	Voltage $U, \text{V}$	Etching rate $V_{er}, \text{mm} / \text{min}$
NaNO <sub>3</sub> – 60; NaNO <sub>2</sub> – 5; Na <sub>2</sub> CO <sub>3</sub> – 5; C <sub>3</sub> H <sub>8</sub> O <sub>3</sub> – 15; H <sub>2</sub> O – rest	30	125	11,5	0,0042

The control point movement of the strain gauges were recorded and the deformation curve was plotted in real time during the layer-by-layer electrochemical etching of the studied surface.

The subsequent information processing (an array of the deformation curves, initial deformations, geometric parameters of the samples) was performed by the XUdion software (a computer program for RS calculation) [15]. The final step of the RS testing was the RS measuring protocol, containing parameters of the sample and the RS epura (RS distribution over the thickness of the removed layer).

The RS calculation in the XUdion software was carried out by a mathematical model for the RS components calculation in the plates using the strip method [16] (Fig. 5):

$$\sigma_Z = \frac{8E}{1-\mu^2} \left( \frac{h}{2} - a \right) V_Z^0 - \frac{4E}{3 \cdot (1-\mu^2)} \left[ (h-a)^2 \frac{dV_Z}{da} - 4(h-a)V_Z + 2 \int_0^a V_Z d\xi \right]; \quad (1)$$

$$\sigma_X = \frac{8E}{1-\mu^2} \left( \frac{h}{2} - a \right) V_X^0 - \frac{4E}{3(1-\mu^2)} \left[ (h-a)^2 \frac{dV_X}{da} - 4(h-a)V_X + 2 \int_0^a V_X d\xi \right]; \quad (2)$$

$$\tau_{ZX} = 2G \left( \frac{h}{2} - a \right) u_\tau^0 - \frac{G}{3} \left[ (h-a)^2 \frac{du_\tau}{da} - 4(h-a)u_\tau + 2 \int_0^a u_\tau d\xi \right]. \quad (3)$$

where  $\sigma_z$  and  $\sigma_x$  are RS normal components, MPa;  $\tau_{zx}$  – RS tangent component, MPa;  $E$  – the elastic modulus, MPa;  $G$  – the shear modulus, MPa;  $\mu$  – Poisson’s ratio;

$$V_z^0 = f_z^0 / l_z^2 + \mu \cdot f_x^0 / l_x^2; V_x^0 = f_x^0 / l_x^2 + \mu \cdot f_z^0 / l_z^2; u_\tau^0 = (\chi_z^0 - \chi_x^0) / 2$$

– reduced displacements after cutting;

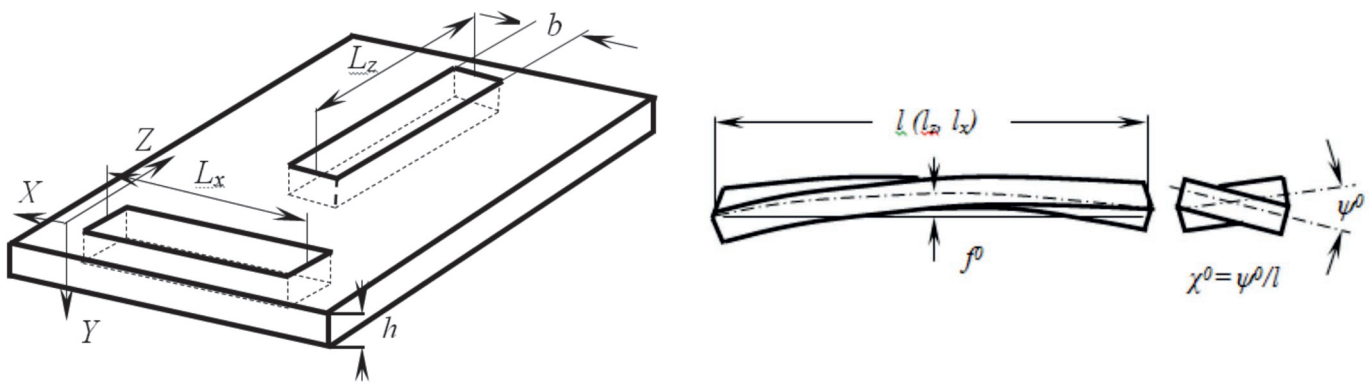


Fig. 5. To an explanation of the formulas for calculating residual stresses by a mechanical method

$$V_z = f_z / l_z^2 + \mu \cdot f_x / l_x^2; V_x = f_x / l_x^2 + \mu \cdot f_z / l_z^2; u_\tau = (\chi_z - \chi_x) / 2$$

– reduced displacements recorded during the etching process;  $f_z^0, f_x^0$  – strip deflections changes caused by notching, mm;  $f_z, f_x$  – the same deflections, registered when removing layers, mm;  $\chi_z^0, \chi_x^0$  – changes in the unit angle of the strip twist caused by the notch, rad / mm;  $\chi_z, \chi_x$  – the same changes, registered when removing layers, mm;  $l_z, l_x$  – corresponding lengths of the strips, mm;  $h$  – the initial plate (strip) thickness, mm;  $a$  – the layer thickness removed at the experiment time, mm;  $\zeta$  – the integration variable.

## Results and discussions

The microhardness, structure, phase composition, and stress state were determined in this study. The metallographic analysis revealed that a diffusion layer of 20  $\mu\text{m}$  thick was formed after boriding at 950  $^\circ\text{C}$  (Fig. 6, *a*). An increase in temperature up to 1050  $^\circ\text{C}$  resulted in a diffusion layer formation up to 105  $\mu\text{m}$  thick (Fig. 6, *b*). Boride layers have a teeth-like structure with rounded ends oriented in the direction of boron diffusion. In the upper part of the layer, pores were observed, which appeared due to interaction with ambient air. After TCT in both temperature modes, a transition zone was formed in a dark area under the borides. In this case, after high-temperature treatment, light crystals oriented along the grain boundaries of the base metal were detected. Probably it was carboborides ( $\text{Fe}_3(\text{B,C})$ ) [17].

The maximum microhardness after treatment at 950  $^\circ\text{C}$  was 1250 HV, at 1050  $^\circ\text{C}$  was 1880 HV corresponding to  $\text{Fe}_2\text{B}$  and  $\text{FeB}$  iron borides (Fig. 7) [1-4]. XRD analysis confirmed the presence of  $\text{Fe}_2\text{B}$  in the diffusion layer after TCT at 950  $^\circ\text{C}$  and  $\text{FeB}$  after TCT at 1050  $^\circ\text{C}$  (Fig. 8). In the first case, a high microhardness gradient was observed between the layer and the base metal reaching 800 HV (Fig. 7, *a*). In the second case, the values smoothly decreased towards the base metal, which is more preferable for the products operating under alternating stress conditions (Fig. 7, *b*).

The second softer  $\text{Fe}_2\text{B}$  boride and a more developed transition zone with carboborides after boriding at 1050  $^\circ\text{C}$  contributed to the smooth microhardness profile.

In order to determine the layer's elemental composition in local areas and separate structural components, the EDS analysis was used (Fig. 9). The results of quantitative analysis are presented in Tables 3 and 4. The low-temperature boriding mode led to the formation of  $\text{Fe}_2\text{B}$  iron boride with the highest boron content of about 6 % in the upper part of the layer (spectrum 1 and a line spectrum 1 on Fig. 9, *a*). The boron content after treatment at 1050  $^\circ\text{C}$  increased up to 11 %. In both temperature modes increased chromium content was revealed, which is associated with the scanning at a relatively low accelerating voltage to detect light elements, for example, boron. The tungsten content in the diffusion layer varied in the range from 1 to 13 %, which indicated its inhomogeneous distribution in the layer. Also, light carbide inclusions up to 1  $\mu\text{m}$  were observed in its microstructure (Fig. 9, *a*).

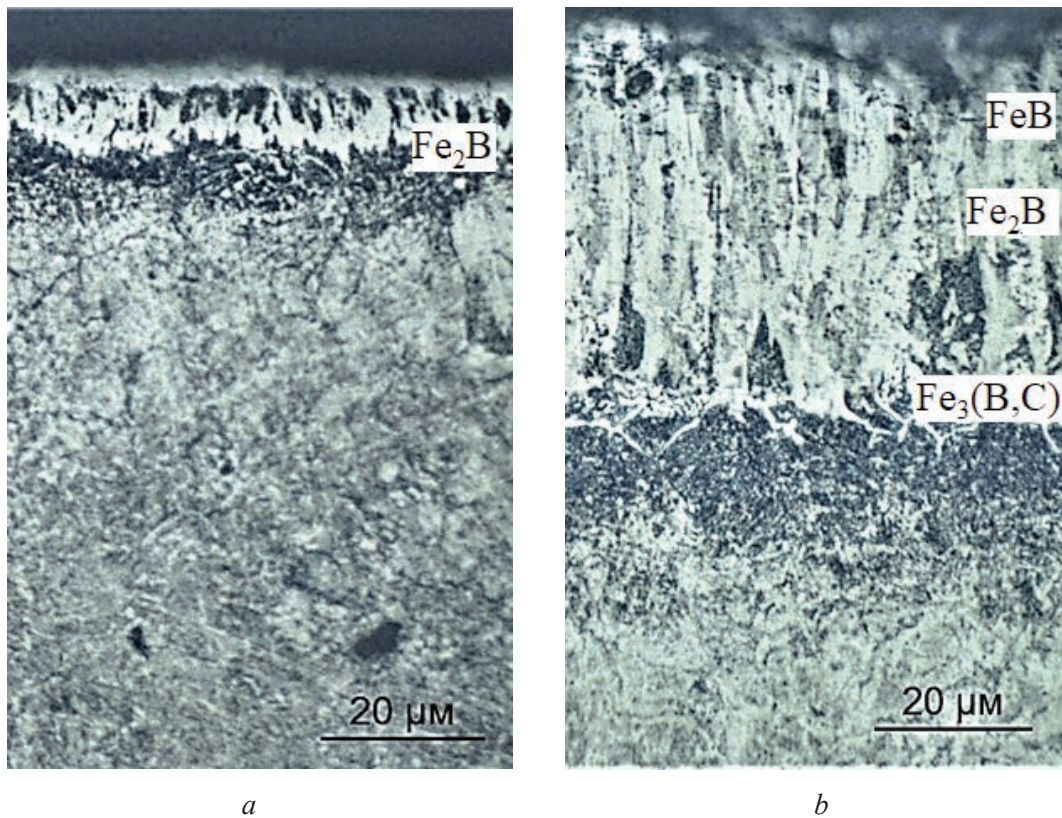


Fig. 6. Microstructures of steel 3Kh2V8F after TCT at temperature:  
*a* – 950 °C; *b* – 1050 °C

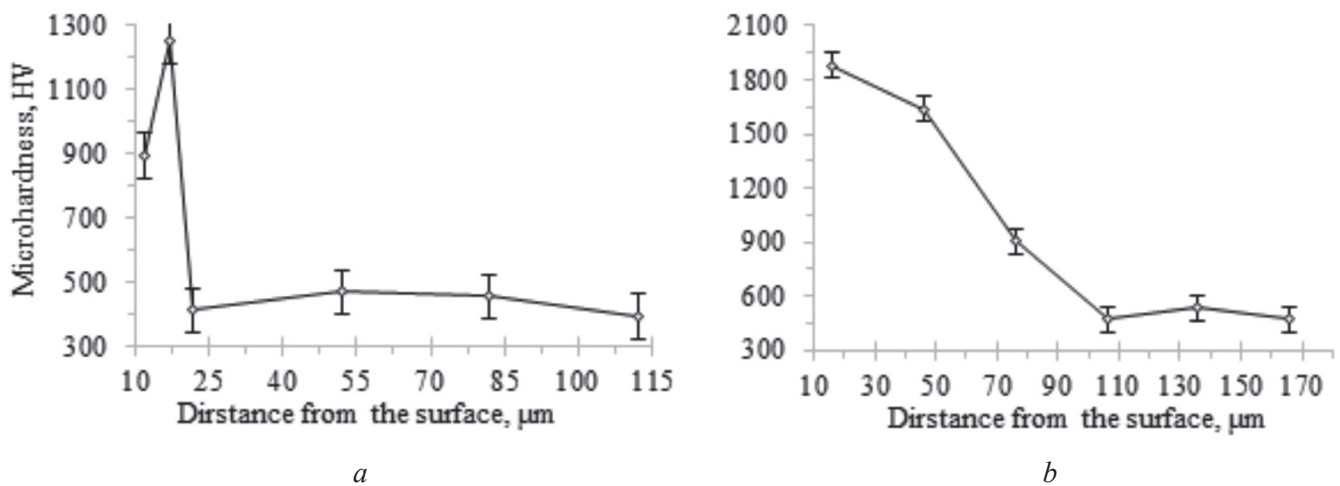


Fig. 7. Depth distribution of microhardness after TCT at temperature:  
*a* – 950 °C; *b* – 1050 °C

Figure 10 shows the strip samples as a result of electrochemical etching (anodic dissolution) after the RS determination on the UDION-2 installation.

Figures 11, 12 show the RS epures based on the experiment result. As it is seen on the diagrams, the normal component of the RS appears due to the diffusion processes occurring throughout the entire base metal and forms a plane stress-strain state of one type. That means any direction is a main one, therefore, it is necessary and sufficient to measure only one normal (main) component of the RS [18].

The obtained data proved that die steel (0.3 % C, 2 % Cr, 8 % W, 0.2 % V) boriding at 950 °C led to compressive RS (Fig. 11). The minimum values of -180 MPa were observed at a distance from the surface of 25...55 μm in transition zone. The active part of the RS epure was estimated at 0.18 mm thickness

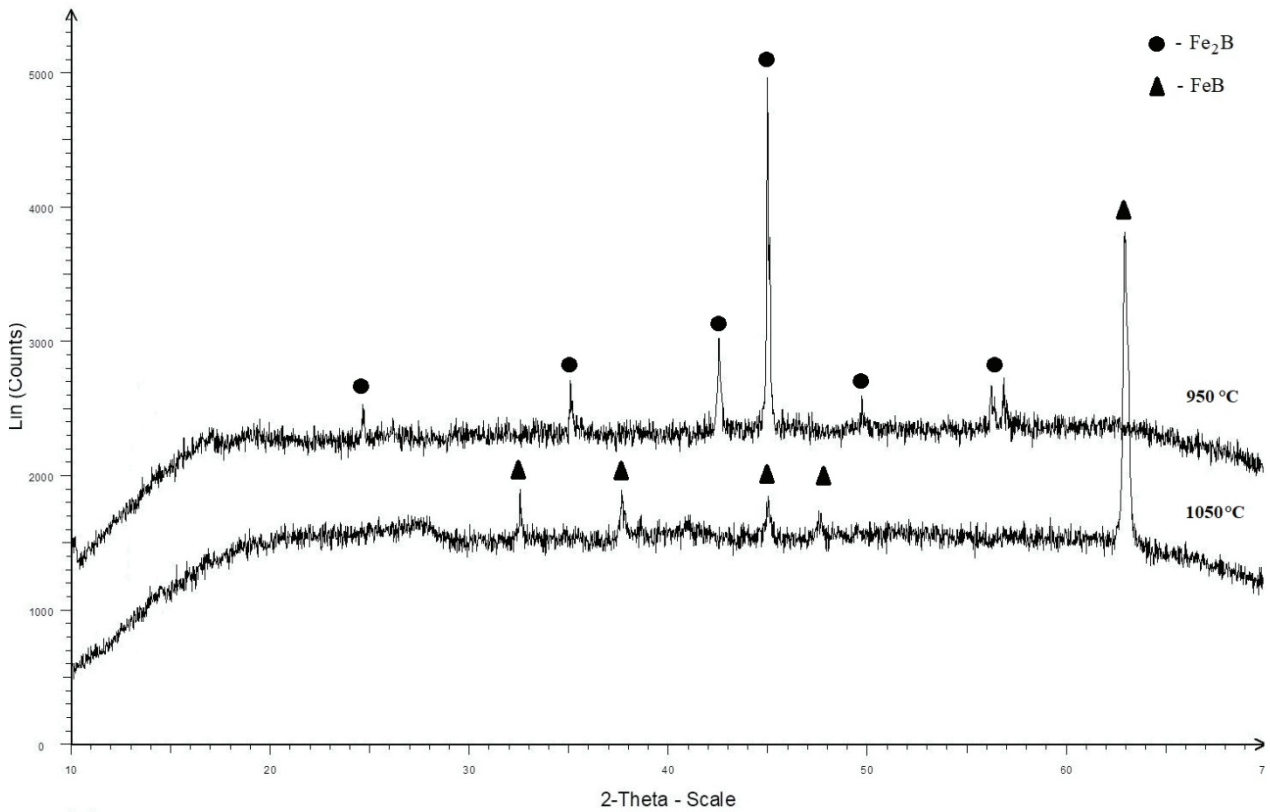


Fig. 8. XRD-pattern of the samples after boriding

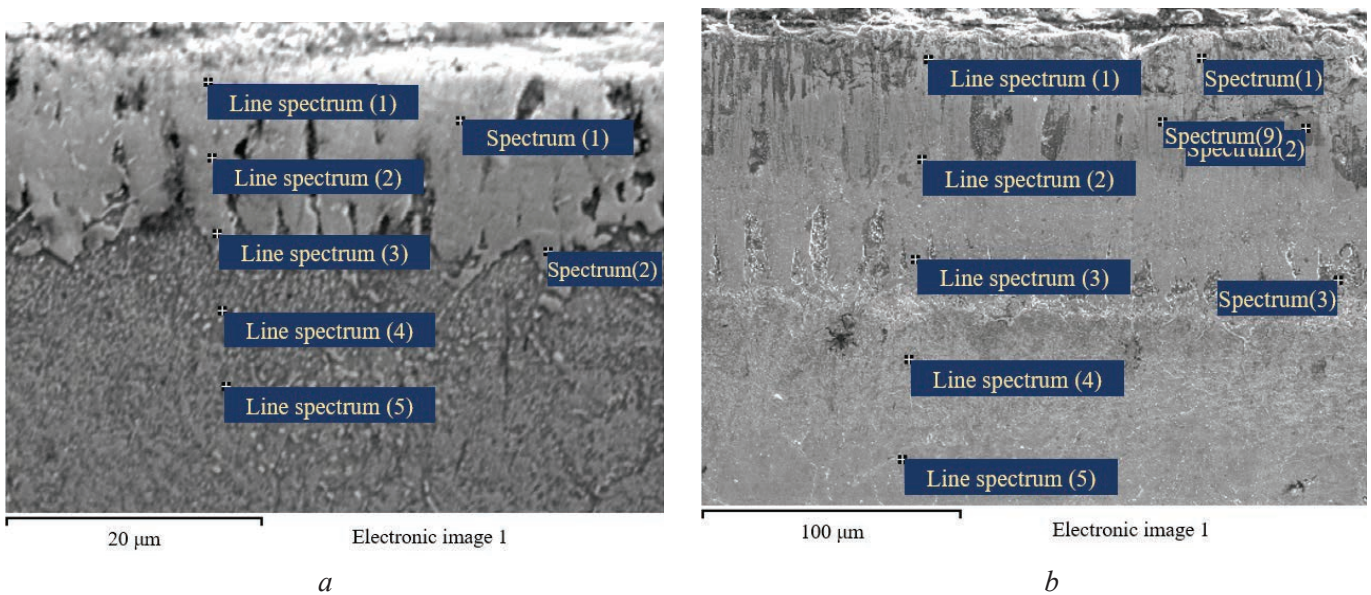


Fig. 9. SEM image of the boride layer:

*a* – 950 °C, 2 h; *b* – 1050 °C, 2 h

from the surface. After boriding at 1050 °C (Fig. 12), tensile RS appeared on the surface with a maximum value of 40 MPa at a distance from the surface of 45 ... 50 µm, and then turned into compressing RS with a minimum value of –124 MPa in the base metal. The active part of the RS epure was rated 0.6 mm from the surface.

The stress state study of the boride layers is only a small part of the reducing brittleness problem related to the FeB/Fe<sub>2</sub>B borides thermal expansion anisotropy and its opposite RS sign. Today, this

Table 3

**Concentration of elements in the surface layer of the sample after TCT at a temperature of 950 °C, wt. % \***

Spectrum No	B	C	V	Cr	Fe	W	Total
Spectrum 1	6	4.9	0.3	8.3	77.8	2.7	100.00
Spectrum 2	–	5.4	0.7	9.3	72.1	12.5	100.00
Line spectrum (1)	6.2	4.3	–	8.8	79.2	1.5	100.00
Line spectrum (2)	1.9	6.1	–	9.8	68.8	13.4	100.00
Line spectrum (3)	3.1	6	–	7.9	80	3	100.00
Line spectrum (4)	–	8	–	11.2	78	2.8	100.00
Line spectrum (5)	–	8.6	–	10.8	72.1	8.5	100.00

\* Quantitative analysis is given to reflect the concentration variation depending on the distance from the surface. The actual values are not possible to define by EDS analysis.

Table 4

**Concentration of elements in the surface layer of the sample after TCT at a temperature of 1050 °C, wt. % \***

Spectrum No	B	C	O	Si	V	Cr	Fe	W	Total
Spectrum 1	10.5	4.5	2.5	–	–	4.1	65.4	13	100.00
Spectrum 2	10.8	5.1	–	–	–	11.3	69	3.8	100.00
Spectrum 3	3.1	4	2.2	0.5	–	6.6	80.8	2.8	100.00
Line spectrum (1)	11.8	3.8	–	–	–	10.7	71.5	2.2	100.00
Line spectrum (2)	1.7	4.8	–	–	0.5	11.3	71.8	9.9	100.00
Line spectrum (3)	3.3	5.5	–	–	–	10.4	74.2	6.6	100.00
Line spectrum (4)	–	7.3	–	–	–	13.5	77.4	1.8	100.00
Line spectrum (5)	–	7.4	–	–	–	10.5	76.7	5.4	100.00
Spectrum 9	–	3.7	–	–	–	12.8	77.7	5.8	100.00

\* Quantitative analysis is given to reflect the concentration variation depending on the distance from the surface. The actual values are not possible to define by EDS analysis.

problem is being solved by the monoboride layer formation consisting of Fe<sub>2</sub>B boride with a developed transition zone. The experiments discovered a single-phase Fe<sub>2</sub>B layer formation after boriding at 950 °C. Although XRD revealed the only FeB phase for high-temperature TCT, the boride layer had a two-phase composition, and Fe<sub>2</sub>B presence was confirmed by numerous reference data and partially including experimental findings, for example, microhardness values [1–4, 19–22]. Thus, two temperature modes of boriding with the same exposure led to the formation of layers with the required phase composition for further RS investigation.

The microhardness distribution pattern correlated well with the RS distribution, for example, high gradients were observed in the diffusion layer and in the adjacent (transition) zone after low-temperature treatment. On the contrary, after boriding at 1050 °C the RS and microhardness distributions over the layer thickness were smoother, except for the transition zone at 105–160 μm distance from the surface, where



Fig. 10. The surface of sample strips as a result of electrochemical etching (anodic dissolution) of samples from steel 3Kh2V8F after boriding at:

*a* – 950 °C; *b* – 1050 °C

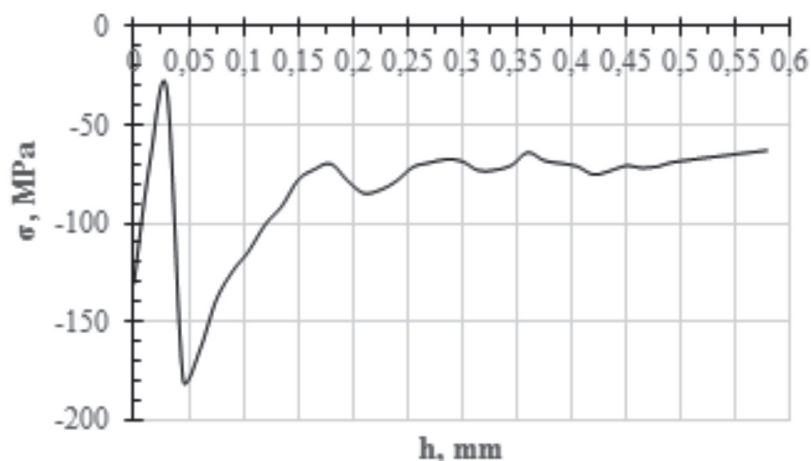


Fig. 11. Diagram of residual stresses in the sample after boriding at 950 °C

the local RS increase was observed (Fig. 12). This increase corresponds to the lowest tungsten content of 1.8 % (a line spectrum 4, Table 4).

The performed study is in good agreement with the current data on die steel (0.3 % C, 2 % Cr, 8 % W, 0.2 % V) boriding in terms of layer thickness, elemental and phase composition, as well as with microhardness values [19]. At the same time, this work is a state-of-the-art for modern RS research, including correlations with the structure and phase composition of the layers. And it should be noted that the upper-temperature limit for the investigated die steel boriding was 50 °C higher than it had been done before [19].

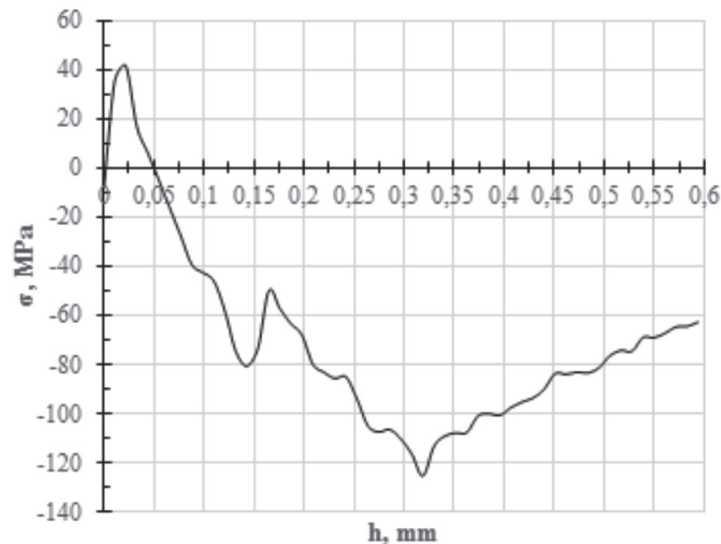


Fig. 12. Diagram of residual stresses in the sample after boriding at 1050 °C

## Conclusion

Thus, boriding at 950 °C is more preferable than boriding at 1050 °C in terms of compressive RS. Nevertheless, significant fluctuations of the RS in the diffusion layer and in the adjacent (transitional) zone may negatively affect the operational properties. Despite the tensile stress on the surface of the diffusion layer after high-temperature TCT, the RS distribution is smoother compared to low-temperature boriding. In addition, the diffusion layer has a greater thickness (up to 100 μm) after high-temperature TCT. It is recommended to apply subsequent finishing treatment (fine grinding) to ensure the performance properties of the surface in a broader range of use (dimensional accuracy, roughness, level and RS sign).

## References

1. Voroshnin L.G., Mendeleeva O.L., Smetkin V.A. *Teoriya i tekhnologiya khimiko-termicheskoi obrabotki* [Theory and technology of chemical and heat treatment]. Moscow, Novoe znanie Publ., 2010. 304 p. ISBN 978-5-94735-149-1.
2. Krukovich M.G., Prusakov B.A., Sizov I.G. Plasticity of boronized layers. *Springer Series in Materials Science*, 2016, vol. 237, pp. 111–227. DOI: 10.1007/978-3-319-40012-9.
3. Kulka M. Trends in thermochemical techniques of boriding. Kulka M. *Current trends in boriding: Techniques*. Cham, Switzerland, Springer, 2019, pp. 17–98. DOI: 10.1007/978-3-030-06782-3\_4.
4. Bel'skii E.I., Sitkevich M.V., Ponkratin E.I., Stefanovich V.A. *Khimiko-termicheskaya obrabotka instrumental'nykh materialov* [Chemical and thermal treatment of tool materials]. Minsk, Nauka i tekhnika Publ., 1986. 247 p.
5. Burkin S.I., Shimov G.V., Andryukova E.A. *Metallurgiya. Ostatochnye napryazheniya v metalloproduktii* [Metallurgy. Residual stresses in metal products]. Moscow, Ekaterinburg, Yurait Publ., 2018. 247 p. ISBN 978-5-534-06500-8.
6. Pishchov M.N., Bel'skii S.E. Analiz ostatochnykh napryazhenii v uprochnennom sloe zubchatykh koles trelevochnogo traktora posle provedeniya khimiko-termicheskoi obrabotki [Analysis of residual stresses in the hardened layer of skidder gear wheels after chemical and thermal treatment]. *Trudy BGTU. Seriya 2, Lesnaya i derevoobrabatyvayushchaya promyshlennost' = Proceedings of BSTU. Series 2, Forest and Woodworking Industry*, 2010, iss. 18, pp. 294–298.
7. Pavlov V.F., Vakuljuk V.S., Afanasieva O.S., Bukatyi A.S. Otsenka vliyaniya khimiko-termicheskoi obrabotki na soprotivlenie ustalosti obraztsov pri normal'noi i povyshennoi temperaturakh [Evaluation of thermochemical treatment influence on fatigue strength of specimens under normal and high temperatures]. *Vestnik Samarskogo gosudarstvennogo aerokosmicheskogo universiteta = Vestnik of Samara State Aerospace University*, 2012, no. 5 (36), pp. 113–119.

8. Sawicki J., Kruszyński B., Wójcik R. The influence of grinding conditions on the distribution of residual stress in the surface layer Of 17CrNi6-6 steel after carburizing. *Advances in Science and Technology Research Journal*, 2017, vol. 11 (2), pp. 17–22. DOI: 10.12913/22998624/67671.
9. Ulakhanov N.S., Mishigdorzhiiyn U.L., Greshilov A.D., Tikhonov A.G., Ryzhikov I.N. Surface processing technology in improving operational properties of hot-work tool steel. *AER-Advances in Engineering Research*, 2019, vol. 188, pp. 362–366. DOI: 10.2991/aviaent-19.2019.67.
10. Nechaev L.M., Fomicheva N.B., Kanunnikova I.Yu., Markova E.V. Vliyanie ul'trazvukovoi obrabotki na fiziko-mekhanicheskie svoystva borirovannogo sloya [Influence of ultrasound treatment on physical and mechanical properties of boronized layer]. *Sovremennye naukoemkie tekhnologii = Modern high technologies*, 2008, no. 9, pp. 16–19.
11. Fedotov N.I., Kharaev Yu.P., Greshilov A.D., Kurkina L.A. Ostatochnye napryazheniya posle KhTO i BUFO [Residual stresses after TCT and BUFO]. *Fundamental'nye problemy sovremennogo materialovedeniya = Basic Problems of Material Science*, 2011, vol. 8, no. 4, pp. 37–39.
12. Sizov I.G., Mishigdorzhiiyn U.L., Polyansky I.P. Boroaluminized carbon steel. *Encyclopedia of Iron, Steel and Their Alloys*. Ed. by R. Colás, G.E. Totten. New York, Taylor and Francis, 2016, pp. 346–357. DOI: 10.1081/e-eisa-120049887.
13. Zamashchikov Yu.I. *Sposob opredeleniya ostatochnykh napryazhenii* [Method for determining residual stresses]. Patent RF, no. 2121666, 1998.
14. Tikhonov A.G., Pashkov A.E. Comparative study of residual stresses when turning HSS-5 steel with varying feed. *IOP Conference Series: Materials Science and Engineering*, 2019, vol. 632, p. 012113. DOI: 10.1088/1757-899X/632/1/012113.
15. Zamashchikov Yu.I., Tolstikhin K.V. *Programmnyi modul' rascheta ostatochnykh napryazhenii po dannym, poluchennym metodom udaleniya sloev* [Software module for calculating residual stresses based on data obtained by the layer removal method]. The Certificate on official registration of the computer program. No. 2015619838, 2016.
16. Zamashchikov Yu.I. Surface residual stress measurements by layer removal method. *International Journal of Machining and Machinability of Materials*, 2014, vol. 16 (3–4), pp. 187–211. DOI: 10.1504/IJMMM.2014.067307.
17. Lentz L., Röttger A., Theisen W. Hardness and modulus of  $\text{Fe}_2\text{B}$ ,  $\text{Fe}_3(\text{C},\text{B})$ , and  $\text{Fe}_{23}(\text{C},\text{B})_6$  borides and carboborides in the Fe-C-B system. *Materials Characterization*, 2018, vol. 35, pp. 192–202. DOI: 10.1002/srin.201000255.
18. Zaides S.A., ed. *Tekhnologiya eksperimental'nykh issledovaniy*. V 2 kn. Kn. 2 [Technology of experimental studies. In 2 bk. Bk. 2]. Irkutsk, Irkutsk State Technical University Publ., 2011, pp. 121–158. ISBN 978-5-8038-0719-3.
19. Voroshnin L.G. *Borirovanie promyshlennykh stalei i chugunov* [Boronizing of industrial steels and cast iron]. Minsk, Belarus' Publ., 1981. 205 p.
20. Jurči P., Hudáková M. Diffusion boronizing of H11 hot work tool steel. *Journal of Materials Engineering and Performance*, 2011, vol. 20, pp. 1180–1187. DOI: 10.1007/s11665-010-9750-x.
21. Campos-Silva I., Palomar-Pardavé M., Pérez Pastén-Borja R., Kahvecioglu Feridun O., Bravo-Bárcenas D., López-García C., Reyes-Helguera R. Tribocorrosion and cytotoxicity of FeB-Fe<sub>2</sub>B layers on AISI 316 L steel. *Surface and Coatings Technology*, 2018, vol. 349, pp. 986–997. DOI: 10.1016/j.surfcoat.2018.05.085.
22. Kartal G., Timur S., Sista V., Eryilmaz O.L., Erdemir A. The growth of single Fe<sub>2</sub>B phase on low carbon steel via phase homogenization in electrochemical boriding (PHEB). *Surface and Coatings Technology*, 2011, vol. 206, pp. 2005–2011. DOI: 10.1016/j.surfcoat.2011.08.049.

## Conflicts of Interest

The authors declare no conflict of interest.

© 2021 The Authors. Published by Novosibirsk State Technical University. This is an open access article under the CC BY license (<http://creativecommons.org/licenses/by/4.0/>).